Lattice Boltzmann simulation of dense gas flows in microchannels

Yong Shi and T. S. Zhao
Department of Mechanical Engineering, The Hong Kong University of Science and Technology, Kowloon, Hong Kong, China

Zhaoli Guo
National Laboratory of Coal Combustion, Huazhong University of Science and Technology, Wuhan 430074, China

(Received 6 August 2006; revised manuscript received 8 March 2007; published 23 July 2007)

It is true that the Knudsen number that characterizes gas flows in microchannels increases to a finite value as the geometric dimension is reduced. However, since the gas in such a flow may retain a small mean free path and a small mean molecular spacing, the gas can still be rather dense in microdevices. Gas flows in microchannels have mainly been studied by molecular dynamics and direct simulation Monte Carlo methods. However, both methods are computationally expensive. In this work, we study dense gas flows in microchannels using an Enskog equation-based lattice Boltzmann Bhatnagar-Gross-Krook model. It is found that a dense gas flowing through a microchannel behaves different than a dilute gas under the same flow conditions.

DOI: 10.1103/PhysRevE.76.016707 PACS number(s): 47.11.−j, 47.61.−k

I. INTRODUCTION

Gas flows in microchannels have been receiving increased attention over the last decade [1,2] with the rapid development of microfabrication technologies. It is found that a gas flowing through a small-sized device exhibits some unusual dynamic behaviors, and the conventional Navier-Stokes equations with the nonslip boundary condition fail to give an accurate description [1,2]. The deviation of gas flows in microchannels from the flows in macrochannels is usually characterized by the Knudsen number, defined as $\mathrm{Kn}=l/h$, with l and h representing the mean free path and the characteristic length of channel, respectively. In the literature, many studies assume that gas flows in microchannels are dynamically similar to rarefied gas flows at high altitudes, if both flows have the same Knudsen number [1]. Based on this assumption, gas flows in microchannels are divided into four flow regimes: the continuum flow regime ($\mathrm{Kn}<0.01$), the slip flow regime ($0.01<\mathrm{Kn}<0.1$), the transitional flow regime ($0.1<\mathrm{Kn}<10$), and the free molecular flow regime ($\mathrm{Kn}>10$), just as those for rarefied gas flows at high altitudes [3]. However, this basic assumption for gas flows in microchannels may be questionable as discussed in the following. In fact, in a general gas system, two other characteristic lengths should also be considered: the molecular diameter σ and the mean molecular spacing δ. The ratio of these two lengths is a criterion to judge whether the gas is dilute or dense. For instance, it has been shown [4] that when $\sigma/\delta<1/7$, the gas can be regarded as sufficiently dilute and its dynamics can be described by the Boltzmann equation [2,5] while when $\sigma/\delta>1/7$, the gas is so dense that its dynamics should be described by the kinetic equations for dense fluids, e.g., the Enskog equation [5]. Kinetic theory also shows that the mean molecular spacing and mean free path are related to the gas density as [1]

$$\delta=(\rho/m)^{-1/3} \tag{1}$$

and

$$l=\frac{m}{\sqrt{2}\pi\rho\sigma^2}, \tag{2}$$

where ρ is the gas density and m is the mass of gas molecule. For rarified gas flows at high altitudes, since the gas density is rather low, the mean free path can increase up to being comparable to or even higher than the macroscopic scale length, and the mean molecular spacing becomes much larger than the molecular diameter $\delta\gg\sigma$. Therefore, in essence, rarefied gas flows at high altitudes are the dilute gas flows with a finite Knudsen number. However, this is not always true for gas flows in microchannels. It is known that the Knudsen number increases to a finite value as the channel's dimension is reduced, but the mean free path and mean molecular spacing can still be very small, $(l,\delta)\sim\sigma$. This indicates that the gas in microchannels can be rather dense. In this case, a simple treatment of gas flows in microchannels as rarefied gas flows is questionable as the gas is not dilute. Therefore, the study of dense gas flows with a finite Knudsen number is needed.

Various numerical methods have been employed to study gas flows with a finite Knudsen number, such as the direct simulation Monte Carlo (DSMC) method [6–8], the information preservation method [2], and the gas kinetic scheme [9]. Recently, the lattice Boltzmann method (LBM), a novel and simple mesoscopic approach, has received particular attention in the study of gas flows in microchannels. In the literature, a number of papers on gas flows in microchannels using the LBM have been reported [10,12–18]. The first lattice Boltzmann Bhatnagar-Gross-Krook (LBGK) model was proposed by Nie *et al.* in 2002 [10]. In their model, they related the Knudsen number Kn with the dimensionless relaxation time τ as $\mathrm{Kn}=a(\tau-0.5)/(\rho h)$. a is an adjustable numerical parameter, whose magnitude is determined by the comparison of the numerical results obtained by the LBGK model with experiment data. Moreover, they directly applied the bounce back rule to model the slip effect between gas molecules and solid wall. It is known that such a mesoscopic boundary condition corresponds to the macroscopic no-slip

boundary condition. Some studies have shown that the slip presented in Ref. [10] is the numerical error of the bounce back rule, different from the actual physical slip [11,14]. Almost at the same time, Lim *et al.* [12] developed another LBGK model, in which Kn is related to τ by assuming that the rate of gas molecules relaxing toward equilibrium is equal to the speed at which the gas molecules travel a grid spacing Δx within a time interval Δt. In their work, Lim *et al.* discussed the numerical results with the specular reflection boundary condition and the extrapolation boundary condition, respectively. To gain a more accurate prediction, the later LBGK studies focused on modifying the boundary condition: Succi [13] proposed a mixed boundary condition combining the bounce back rule with the specular reflection scheme; Lee and Lin [14] devised a wall equilibrium boundary condition to model the interaction between gas molecules and fully diffusive reflected walls; Ansumali and Karlin [15] developed a discrete kinetic boundary condition based on the Maxwell's diffusion reflection boundary condition in kinetic theory. Tang *et al.* [16] later combined this kinetic boundary condition with the specular reflection boundary condition to simulate the micro-Couette flow, the micro-Poiseuille flow, and the microcavity flow. Recently, Guo *et al.* [17] studied systemically the applicability of the present LBGK models for gas flows in microchannels, and developed a LBGK model with consideration of the wall effect on the relaxation time; Kim *et al.* [18] constructed one model in which they introduced two relaxation times to give rise to two different viscosities in the Knudsen layer and the bulk flow region, respectively. The basic idea of this two-relaxation time LBGK model is that although being quite different from the bulk flow, the flow in the Knudsen layer may still be described by the conventional Navier-Stokes equations provided that the fluid properties are appropriately specified. Nevertheless, their model involves many unknown parameters. Determination of these parameters requires knowing the flow details beforehand. Therefore, their model is useful for some particular simple flows, e.g., the Poiseuille flow, which has already been well solved by other theoretic and numerical studies [19]. Different as the details in these LBGK studies are, previous studies show that the lattice Boltzmann method can give a fairly good description of gas flows in the slip flow regime, and may qualitatively capture the fundamental flow behaviors in the transitional flow regime.

On the other hand, it should be pointed out that these existing LBGK studies are limited to dilute gas flows with a finite Knudsen number, as they are based on the Boltzmann equation [20,21]. To gain a deeper insight of gas flows in microchannels, it is essential to develop a LBGK model for simulation of dense gas flows with a finite Knudsen number. To this end, in this paper, we present a finite difference LBGK model based on the Enskog equation for dense gas flows in microchannels in the slip flow regime. The proposed model is developed from our recent work [22]. Unlike those Boltzmann equation-based models, the model takes account of the dense effect due to the finite size of gas molecules. It not only gives the equation of state and transport properties, but also recovers the original expression of viscosity in terms of the Knudsen number in kinetic theory of dense gases.

The rest of the paper is organized as follows. In Sec. II, we first briefly review the basic results of dense gases resulted from kinetic theory. In Sec. III, we present the finite difference Enskog equation-based lattice BGK (ELBGK) model for dense gas flows in microchannels. In Sec. IV, numerical simulations of gas flows with different Knudsen numbers and length ratios, σ/δ, are performed, and the numerical results are analyzed and discussed. Finally, some conclusions are drawn in Sec. V.

II. KINETIC THEORY FOR DENSE GASES

As the mean molecular spacing of a gas is reduced and becomes comparable to its molecular diameter, the gas system is dense and the Boltzmann equation becomes insufficient [4]. Alternatively, the Enskog equation is a well-accepted kinetic theory for such dense gas systems [5,23]. However, the original Enskog equation is rather complicated, and in practical applications it is often simplified as a BGK-like model [24,25]:

$$\frac{\partial f}{\partial t} + \mathbf{c} \cdot \frac{\partial f}{\partial \mathbf{r}} = -\frac{\chi}{\lambda'}(f - f^{\mathrm{eq}}) + J, \tag{3}$$

where

$$\lambda' = \lambda[1 + 2b\rho\chi/(D+2)]^2 \tag{4}$$

and

$$J = -f^{\mathrm{eq}} b\rho\chi(\mathbf{c} - \mathbf{u}) \cdot \frac{\partial}{\partial \mathbf{r}} \ln(\rho^2\chi), \tag{5}$$

f is the singlet distribution function; t, $\mathbf{r}$, and $\mathbf{c}$ denote the time, particle position, and particle velocity, respectively; λ is the relaxation time for dilute gases, and the local equilibrium distribution function f^{eq} is given as

$$f^{\mathrm{eq}} = \rho(2\pi RT_0)^{-D/2}\exp[-(\mathbf{c} - \mathbf{u})^2/(2RT_0)], \tag{6}$$

with D, R, $\mathbf{u}$, and T_0 representing the space dimension, the gas constant, the fluid velocity, and the reference temperature, respectively. Moreover, χ is the pair correlation function and can be expressed as a polynomial of the fluid density [5]

$$\chi = 1 + \frac{5}{8}b\rho + 0.2869(b\rho)^2 + 0.1103(b\rho)^3 + 0.0386(b\rho)^4, \tag{7}$$

with $b = 2\pi\sigma^3/(3m)$. Note that in comparison with the Boltzmann equation with the BGK approximation [2,5], Eq. (3) introduces a new relaxation time λ' and a source term of J to describe the dense effect arising from the finite size of gas molecules. Through the Chapman-Enskog procedure, it can be demonstrated that Eq. (3) recovers the Navier-Stokes equations with the dense gas equation of state

$$p = \rho RT_0(1 + b\rho\chi) \tag{8}$$

and the shear viscosity

$$\mu = \mu^{id}[1 + 2b\rho\chi/(D+2)]^2/\chi, \tag{9}$$

where μ^{id} is the shear viscosity of the corresponding dilute gases. It should be pointed out that the original Enskog theory actually leads to two viscosities for a compressible isotropic Newtonian fluid flow, i.e., the shear viscosity μ and the bulk viscosity μ' [5]. However, for dense gases, since the bulk viscosity μ' is very small, it can be neglected. This is the so-called Stokes hypothesis [26]. Following this idea, we do not consider the bulk viscosity of dense gas in the present study.

The Knudsen number Kn for a gas system is defined as

$$\mathrm{Kn} = \frac{l}{h} \tag{10}$$

and the mean free path l is related with the relaxation time λ by

$$l = \lambda c^*, \tag{11}$$

where $c^* = \sqrt{\pi RT_0/2}$ is the average velocity characterizing the thermal motion of gas molecules [17]. Moreover, the viscosity of a dilute gas can be obtained from the Boltzmann theory [5]:

$$\mu^{id} = \rho RT_0\lambda. \tag{12}$$

Therefore, from Eqs. (10)–(12), the viscosity of a dense gas can be rewritten in terms of the Knudsen number as

$$\mu = \rho RT_0 \mathrm{Kn}\, h[1 + 2b\rho\chi/(D+2)]^2/(\chi c^*). \tag{13}$$

III. FINITE DIFFERENCE ENSKOG EQUATION-BASED LBGK MODEL

In this section, we develop a finite difference LBGK model based on Eq. (3) to simulate dense gas flows in microchannels. Without loss of generality, we focus on two dimensional problems ($D=2$).

We first discretize the particle velocity space into a discrete velocity set $\{\mathbf{c}_i\}$ given by [27]

$$\mathbf{c}_i = \begin{cases} (0,0), & i = 0, \\ c\{\cos[(i-1)\pi/2], \sin[(i-1)\pi/2]\}, & i = 1,2,3,4, \\ \sqrt{2}c\{\cos[(2i-9)\pi/4], \sin[(2i-9)\pi/4]\}, & i = 5,6,7,8, \end{cases} \tag{14}$$

with the speed $c = \sqrt{3RT_0}$. With these discrete velocities, Eq. (3) is reduced to

$$\frac{\partial f_i}{\partial t} + \mathbf{c}_i \cdot \frac{\partial f_i}{\partial \mathbf{r}} = -\frac{\chi}{\lambda'}(f_i - f_i^{\mathrm{eq}}) + J_i, \tag{15}$$

where

$$J_i = -f_i^{\mathrm{eq}} b\rho\chi(\mathbf{c}_i - \mathbf{u}) \cdot \frac{\partial}{\partial \mathbf{r}} \ln(\rho^2\chi), \tag{16}$$

and the discrete velocity local equilibrium distribution function f_i^{eq} is given by

$$f_i^{\mathrm{eq}} = w_i\rho\left(1 + \frac{\mathbf{c}\cdot\mathbf{u}}{c_s^2} + \frac{(\mathbf{c}\cdot\mathbf{u})^2}{2c_s^4} - \frac{\mathbf{u}^2}{2c_s^2}\right), \tag{17}$$

with the sound speed $c_s = \sqrt{3}c/3$, the weight coefficients $w_0 = 4/9$; $w_i = 1/9$, for $i = 1,2,3,4$; and $w_i = 1/36$, for $i = 5,6,7,8$. The gas density and velocity are defined as

$$\rho = \sum_{i=0}^{8} f_i, \quad \rho\mathbf{u} = \sum_{i=0}^{8} f_i\mathbf{c}_i. \tag{18}$$

Next, we apply the general propagation scheme [28] to discretize Eq. (15). The reason why we introduce the finite difference technique in the present study is because in comparison with those conventional ELBGK models [24,25], the resulting finite difference ELBGK algorithm can retain good numerical stability in a much wider range of the length ratios σ/δ. As pointed out in Ref. [22], this improved stability of the present ELBGK model is attributed to the increased hyperviscosity as a result of utilizing the finite difference scheme [29]. The detailed discretization procedure to Eq. (15) is similar to that presented in Ref. [22]. However, it should be pointed out that the model reported in Ref. [22] is for flows with small Knudsen numbers ($\mathrm{Kn} \to 0$). It cannot be directly applied to dense gas flows in microchannels that possess a finite Knudsen number, because such a model gives a viscosity as

$$\mu = \rho RT_0\Delta t[(1 + 2b\rho\chi/(D+2))^2\lambda/(\Delta t\chi) + d/(2A^2) - 1], \tag{19}$$

which includes a discrete error $\Delta = \rho RT_0\Delta t[d/(2A^2) - 1]$, where A and d are two numerical parameters. Therefore, it is expected that when we apply that model in Ref. [22] to simulate dense gas flows in microchannels at a given finite Knudsen number, it will predict a false viscosity different from that of Enskog theory.

To remove such a numerical error, we propose a different finite difference ELBGK model in the present work, which reads

$$\tilde{h}_i^+(t,\mathbf{r}) = \tilde{h}_i(t,\mathbf{r}) - \chi\omega[\tilde{h}_i(t,\mathbf{r}) - \tilde{h}_i^{\mathrm{eq}}(t,\mathbf{r})] + \Delta t J_i, \tag{20}$$

$$\tilde{h}_i(t+\Delta t,\mathbf{r}) = \tilde{h}_i^+(t,\mathbf{r}) + \frac{d}{2}[\tilde{h}_i^+(t,\mathbf{r} + \mathbf{c}_i\Delta t/A) - 2\tilde{h}_i^+(t,\mathbf{r}) + \tilde{h}_i^+(t,\mathbf{r} - \mathbf{c}_i\Delta\mathbf{t}/A)]$$

$$- \frac{A}{2}[\tilde{h}_i^+(t,\mathbf{r} + \mathbf{c}_i\Delta t/A) - \tilde{h}_i^+(t,\mathbf{r} - \mathbf{c}_i\Delta t/A)], \tag{21}$$

where

$$\tilde{h}_i = f_i - 0.5\Delta t J_i + \frac{\chi\Delta t}{2\lambda(1 + 0.5b\rho\chi)^2}(f_i - f_i^{\mathrm{eq}}) \tag{22}$$

and the dimensionless collision frequency ω in Eq. (20) is given by

$$\omega = \frac{\Delta t}{\lambda(1+0.5b\rho\chi)^2 + 0.5\chi\Delta t}. \tag{23}$$

In Eq. (21), we choose $d=A^2$ so that Eq. (21) reduces to the so-called Lax-Wendroff scheme [28,30]. In this finite difference ELBGK model, the gas density and velocity are defined in terms of $\tilde{h}_i$ as

$$\rho = \sum_{i=1}^{8} \tilde{h}_i, \quad \rho\mathbf{u} = \sum_{i=1}^{8} \tilde{h}_i\mathbf{c}_i - \frac{\Delta t}{2} bc_s^2 \frac{\partial}{\partial \mathbf{r}}(\rho^2 g). \tag{24}$$

It can be demonstrated that through the Chapman-Enskog procedure, Eqs. (20) and (21) recover the Navier-Stokes equations with the equation of state and transport properties for dense gases given by

$$p = \rho RT_0(1+b\rho\chi), \tag{25}$$

and

$$\mu = \rho c_s^2 \Delta t\left(\frac{1}{\omega\chi} - \frac{1}{2}\right) = \frac{\mu^{id}}{\chi}(1+0.5b\rho\chi)^2. \tag{26}$$

In order to apply the model to gas flows in microchannels, the collision frequency ω should be related to the Knudsen number. This can be achieved based on the relation between the Boltzmann relaxation time λ and the Knudsen number Kn given by Eqs. (10), (11), and (23), which gives

$$\omega = \frac{\Delta t c^*}{\mathrm{Kn}\, h(1+0.5b\rho\chi)^2 + 0.5\chi\Delta t c^*}. \tag{27}$$

With Eq. (27), we can determine the dimensionless collision frequency ω in Eq. (20) by the given Kn and gas properties.

Another key point to apply the LBGK model to gas flows in microchannels is the realization of the slip boundary condition at solid walls. Although several treatments have been proposed in previous studies [13–16], these methods cannot be applied to the present model directly because they require knowing the unknown distribution functions inside the solid wall. Moreover, those reported discrete kinetic boundary conditions, e.g., the Maxwell diffusive boundary condition [15–17,31,37], may become invalid for dense gas flows in microchannels since they are derived based on the low density limit [32]. Alternatively, we use a second-order slip boundary condition that models the interactions between gas molecules and solid wall [1]. For a fully diffusive reflected wall, it gives

$$u_f - u_w = c_1 l\left(\frac{\partial u}{\partial n}\right)_w + c_2 l^2\left(\frac{\partial^2 u}{\partial n^2}\right)_w, \tag{28}$$

where n is the coordinate in the direction normal to the wall, u_f is the streamwise fluid velocity on the wall, and u_w is the wall velocity. c_1 and c_2 are two coefficients. They have different values in different studies. In the present work, as suggested by Ref. [1], we choose $c_1=1.0$ and $c_2=0.5$. Equation (28) can be written in a dimensionless form as [1]

$$U_f - U_w = c_1 \mathrm{Kn}\left(\frac{\partial U}{\partial n}\right)_w + c_2 \mathrm{Kn}^2\left(\frac{\partial^2 U}{\partial n^2}\right)_w, \tag{29}$$

where U_f and U_w are, respectively, the dimensionless fluid velocity and wall velocity, normalized by a reference velocity. With Eq. (28), we can calculate the distribution function f_i at boundary nodes by the nonequilibrium extrapolation scheme [33]:

$$f_i(t,\mathbf{r}_w) = f_i^{\mathrm{eq}}(t,\mathbf{r}_w;\rho_f,u_f) + [f_i(t,\mathbf{r}_f) - f_i^{\mathrm{eq}}(t,\mathbf{r}_f)], \tag{30}$$

where ρ_f is the gas density at the solid wall, $f_i(t,\mathbf{r}_w)$ and $f_i(t,\mathbf{r}_f)$ are the distribution functions at the solid wall and at the node in the flow region near the wall, respectively. However, note that the distribution function used in the present model, i.e., Eqs. (21) and (22), is a redefined one $\tilde{h}_i$, instead of the original f_i. Therefore, we propose the following procedure to obtain the gas density and velocity based on these two distribution functions, $\tilde{h}_i$ and f_i.

(1) Update the distribution functions $\tilde{h}_i$ in the internal flow field by Eqs. (20) and (21) and calculate the corresponding distribution functions f_i by Eq. (22).

(2) Update the distribution functions f_i at the boundary nodes by Eq. (30).

(3) Calculate the gas density in the entirely flow field and the gas velocity at boundary nodes with f_i by Eq. (18). With the updated gas density, calculate the density gradient in the entire flow field.

(4) Calculate the gas velocity in the internal flow field with $\tilde{h}_i$ and the density gradient by Eq. (24).

With these four steps, we can update the gas densities and velocities in the entire flow field at every time step.

In summary, Eqs. (20)–(24), together with Eqs. (17) and (18), form a finite difference ELBGK model for dense gas flows in microchannels. In the next section, we shall apply this model, along with the boundary condition (29) and (30), to simulation of dense gas flows in microchannels with different Knudsen numbers and length ratios σ/δ.

IV. NUMERICAL SIMULATIONS

A. Validation

We first validate the present model by simulating of a dilute air flow in a microchannel with height H_0 and length L_0. The flow is driven by a pressure gradient imposed at both ends of the channel, and the air at the outlet is under the atmospheric condition and its properties were evaluated at the temperature $T_0=298$ K, which gives $\sigma/\delta=0.0969$. The walls of channel are assumed to be fully diffusive (the accommodation coefficient $\alpha=1$). In order to compare the numerical results with those obtained by the DSMC method [34], we set the length ratio $L_0/H_0=100$, the ratio of the inlet pressure to the outlet pressure $rp=p_i/p_o=1.4$. In simulations, the Knudsen number at the outlet Kn_o is set to be 0.0194, indicating that the flow is in the slip flow regime.

We carried out the simulations on a $N_x \times N_y = 2000 \times 20$ grid and applied the pressure boundary conditions [35] to the

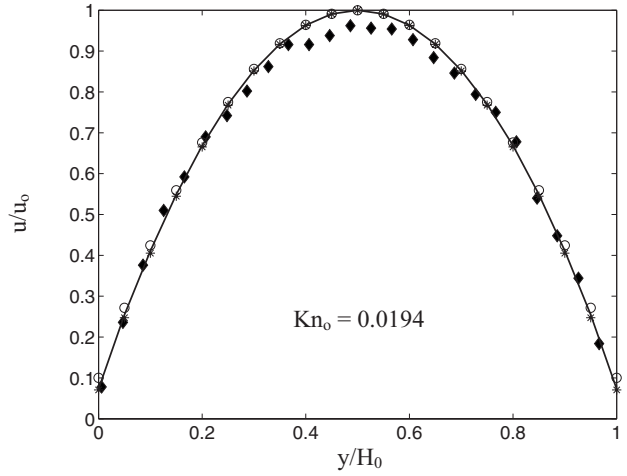

FIG. 1. The streamwise velocity at the outlet of the channel. Solid line: the ELBGK model; ○: the Boltzmann equation-based LBGK model; ♦: the DSMC method; *: the Navier-Stokes equations with the second order slip boundary condition.

inlet and outlet. Moreover, the nonequilibrium extrapolation scheme (30) combined with the slip boundary condition (29) is employed to specify the distribution functions on the solid wall.

Figure 1 presents the streamwise velocity profile across the channel at the outlet when $\mathrm{Kn}_o=0.0194$, where the velocity is normalized by the maximal outlet streamwise velocity u_o. It is observed that an apparent velocity slip occurs on the solid wall and such a slip velocity is about one tenth of u_o. For comparison, we solved the Navier-Stokes equations with the second order slip boundary condition (28) using the perturbation method in Ref. [36]. We obtain

$$U = \frac{dP/dX[1-4(Y-0.5)^2+4\mathrm{Kn}_o/P-4\mathrm{Kn}_o^2/P^2]}{dP_o/dX[1+4\mathrm{Kn}_o-4\mathrm{Kn}_o^2]} \quad (31)$$

and

$$P^2+12\mathrm{Kn}_oP-12\mathrm{Kn}_o^2\ln P+A_PX+B_P=0, \quad (32)$$

where

$$A_P=rp^2+12\mathrm{Kn}_orp-12\mathrm{Kn}_o^2\ln rp-12\mathrm{Kn}_o-1, \quad (33)$$

$$B_P=12\mathrm{Kn}_o^2\ln rp-rp^2-12\mathrm{Kn}_orp, \quad (34)$$

$X=x/L_0$, $Y=y/H_0$, the dimensionless velocity $U=u/u_o$, and the dimensionless pressure $P=p/p_o$. We numerically solved Eqs. (31) and (32) by the Newtonian iteration scheme, and plotted the resulting velocity profile in Fig. 1. In addition, we also present the numerical results obtained by the DSMC method [34] and the conventional Boltzmann equation-based LBGK model with the discrete kinetic boundary condition [15–17,37] in Fig. 1. As seen, the velocities obtained by the two LBGK models are almost identical, being in good agreement with the Navier-Stokes solver (31) and those by the DSMC method [34].

To more clearly examine the numerical accuracy of the proposed ELBGK model, we further performed the grid convergence test. We carried out the simulations on the $N_x \times N_y=1000\times10$, 2000×20, and 4000×40 grids, respectively. The resulting streamwise velocity profiles at the outlet are shown in Fig. 2(a). It is found that the numerical results on the 1000×10 grid deviate from those on the finer grids while the numerical results on the 2000×20 grid is almost identical to those on the 4000×40 grid, indicating that the 2000×20 grid is sufficient for the present case. We also measured the errors of these simulations. Since there is no analytical solution to the dilute air flows in microchannels, we applied the Richardson extrapolation to define an "exact" solution based on the results on the 2000×20 grid and the 4000×40 grid, as discussed in Ref. [38]. The L_1-norm of error [38] for the streamwise velocity at the outlet are shown in Fig. 2(b). Apparently, the results demonstrate that the proposed ELBGK model is of the second-order accuracy.

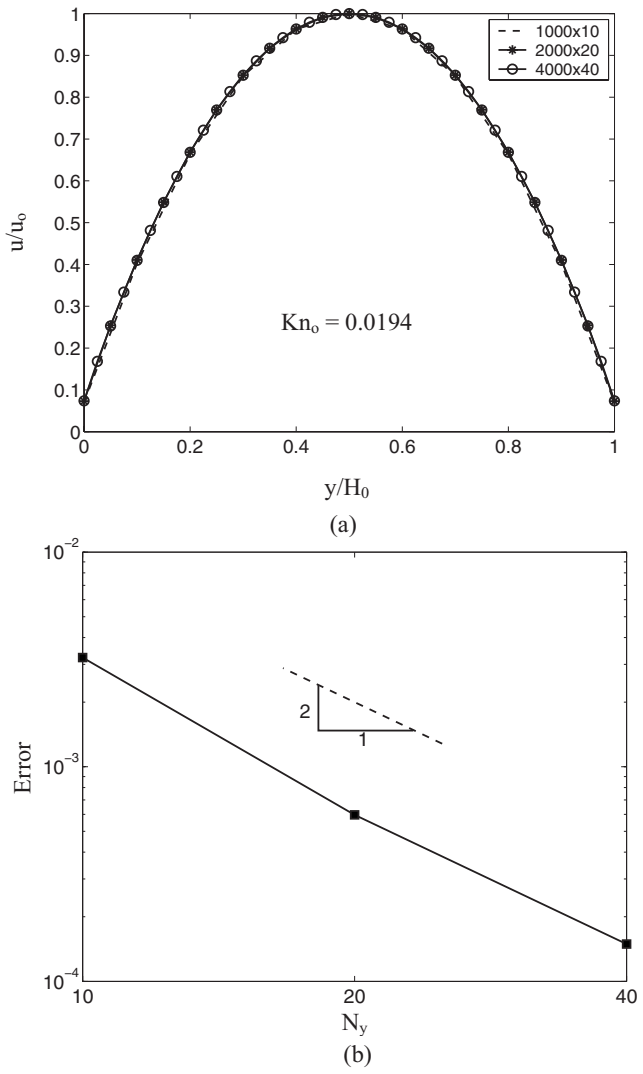

FIG. 2. The grid convergence test of the proposed ELBGK model. (a) The streamwise velocity at the outlet of the channel simulated on the $N_x\times N_y=1000\times10$, 2000×20, 4000×40 grids. (b) Errors comparison in different grids.

In addition to the gas velocity, another interesting point of gas flows in microchannels is the pressure distribution along

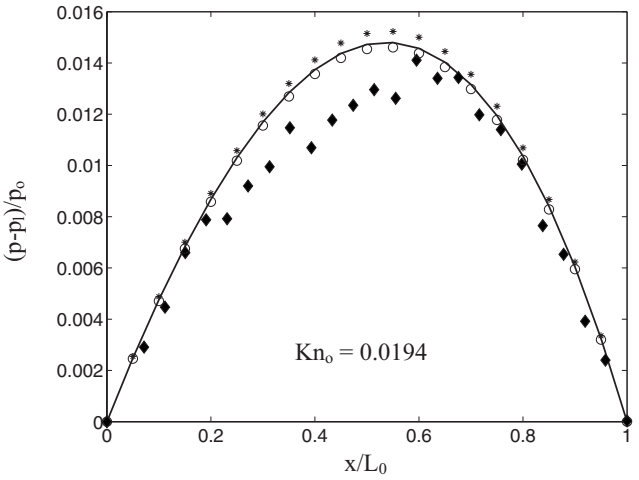

FIG. 3. The pressure deviation from the linear distribution along the channel. Solid line: the ELBGK model; ○: the Boltzmann equation-based LBGK model; ♦: the DSMC method; * the Navier-Stokes equations with the second order slip boundary condition.

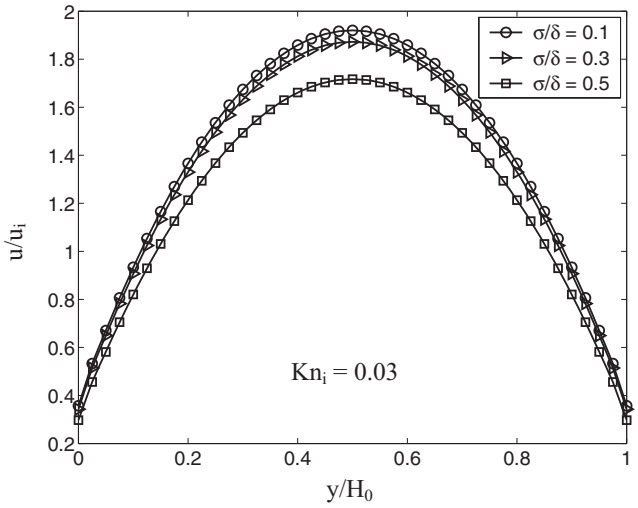

FIG. 4. The streamwise velocity at the outlet of the channel.

channel. It is known that in gas flows in microchannels, the pressure gradient is no longer a constant, but varies along channel. The nonlinear deviation from the linear pressure distribution is due to the compressibility and rarefaction of the gas when it flows through the microchannel [1]. Figure 3 shows the deviations of the nonlinear pressure from the linear distribution along channel predicted by the present ELBGK model, the conventional Boltzmann equation-based LBGK model, the DSMC method [34], and the Navier-Stokes equations with the slip boundary conditions, respectively. As with the gas velocity, the numerical results obtained by the two LBGK models are well agreed with the DSMC method [34]. They all show a convex-curved pressure distribution along channel in the gas flow with $\mathrm{Kn}_o = 0.0194$. However, an overestimation is observed in the results given by Eq. (32). The reason for this overestimation is that the results given by Eq. (32) are only the zeroth-order solution of the Navier-Stokes equations with the second-order slip boundary condition.

B. Simulations of dense gas flows in microchannels

We now apply the proposed finite difference ELBGK model to the study of dense gas flows in a two-dimensional microchannel with the length ratio $L_0/H_0=30$. In our simulations, we chose the Knudsen number at the inlet $\mathrm{Kn}_i = 0.03$, and the pressure ratio $p_i/p_o=2.0$. The temperature of the system is fixed at $T_0=298$ K, and the Courant-Friedricks-Lewey number in the model is set to be $A=0.6$. The boundary conditions are the same as those used in Sec. IV A. For accuracy, the numerical simulations are carried out on a $N_x \times N_y = 1200 \times 40$ grid and three cases with $\sigma/\delta=0.1$, 0.3, and 0.5 are studied.

Figure 4 shows the resulting outlet streamwise velocities, normalized by the maximal inlet velocity u_i. It is seen that the velocities vary sharply in the three cases considered. Specifically, the dense gas with a larger σ/δ always has a smaller gas velocity profile in the bulk flow region and a smaller slip velocity on the solid wall. For instance, when $\sigma/\delta=0.5$, the magnitude of the velocity at the channel center and that on the solid wall decrease, respectively, by 10.59 and 16.72 % in comparison with those in the case of $\sigma/\delta = 0.1$. This behavior is also found by the DSMC method [7].

The velocity slippage at the solid wall along channel is also measured in each case. As shown in Fig. 5, the magnitude of the velocity slip in all the cases increases along the channel. It is also observed that the degree of slip has a clear dependence on the length ratio σ/δ: a dense gas with a larger σ/δ usually gives a smaller slip. For instance, as pointed out previously, the slip velocity at the outlet for $\sigma/\delta=0.5$ decreases 16.72% than that for $\sigma/\delta=0.1$. Such a slip behavior can be analyzed based on the employed boundary conditions. As shown by Eq. (28) or (29), the slip velocity is closely related to the local Knudsen number Kn, which is a function of the gas density. Actually, as shown in Fig. 6, for a given Knudsen number at the inlet, the local Knudsen number in-

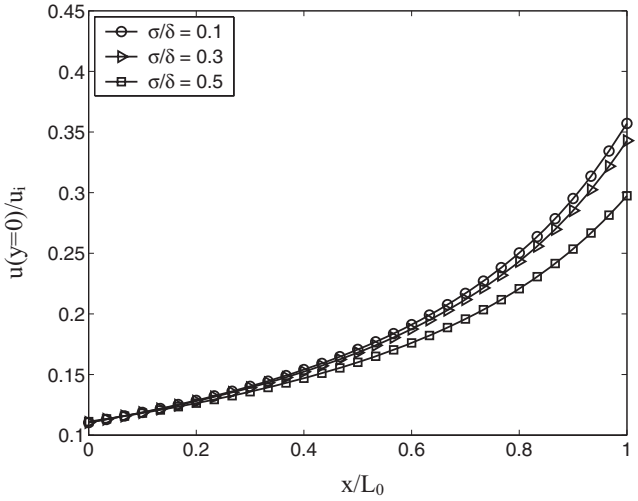

FIG. 5. The slip velocity along the channel when $\mathrm{Kn}_i=0.03$.

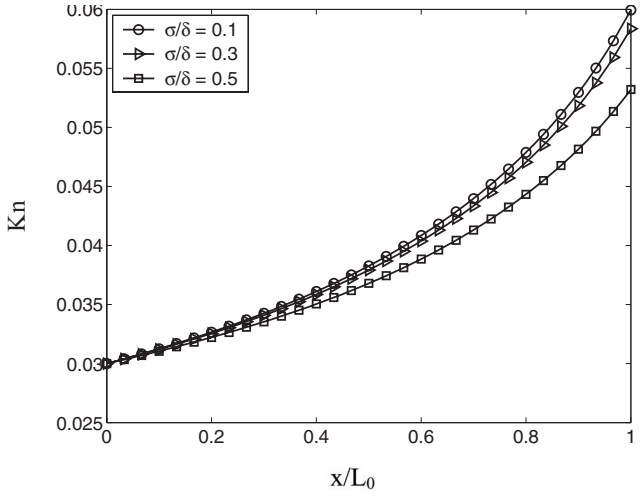

FIG. 6. The variation of the local Knudsen number along the channel when $Kn_i=0.03$.

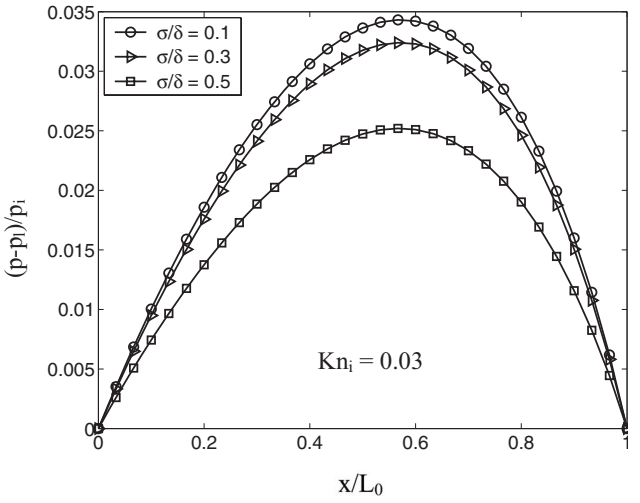

FIG. 7. The pressure deviation from the linear distribution along the channel.

creases along the channel, and at the same position, Kn has a smaller value for a denser gas than that for a less dense one. The reason for small local downstream Knudsen numbers in dense gas flows in microchannels can be explained as follows. For a gas, the local Knudsen number is conversely proportional to the local density $\mathrm{Kn} \propto 1/\rho$. However, as driven by an identical pressure drop, a denser gas (referred to as 1) has a relatively smaller density variation than a less dense one (referred to as 2) [22], i.e.,

$$\left(\frac{\rho_{\mathrm{in}}}{\rho}\right)_1 < \left(\frac{\rho_{\mathrm{in}}}{\rho}\right)_2, \tag{35}$$

where ρ_{in} is the inlet gas density, ρ is the local downstream gas density. As such, the local Knudsen number of the denser gas is smaller than that of the less dense one:

$$\left(\frac{\mathrm{Kn}}{\mathrm{Kn}_{\mathrm{in}}}\right)_1 < \left(\frac{\mathrm{Kn}}{\mathrm{Kn}_{\mathrm{in}}}\right)_2. \tag{36}$$

The pressure distributions for the three cases are shown in Fig. 7. Similar to the validation case, the pressure distributions also deviate from the linear distribution in all the cases. Furthermore, like the distributions of the velocity, the magnitude of the nonlinear deviation also depends on the length ratio σ/δ: it is gradually decreased as the σ/δ increases. Such a tendency may also be attributed to the relatively smaller density variation for a denser gas than that for a less dens gas under an identical pressure drop.

To gain a more complete picture of dense gas flows in microchannels, we also carried out a series of numerical simulations with different Knudsen numbers ranging from 0.01 to 0.04 and different length ratios σ/δ=0.1, 0.3, 0.5. Figure 8 presents the resulting slip velocities at the outlet under different conditions. It is found that for a gas with a given σ/δ, the slip velocities always increase with the Knudsen number, which is consistent with our common understanding in kinetic theory of dilute gases. However, it is also seen that the increased magnitude depends on the length ratio σ/δ. As with previous results, for a given Knudsen number, a larger length ratio results in a smaller slip velocity. The dual dependence of gas slip on both Knudsen number and length ratio σ/δ shows that the actual gas flows in microchannels are determined not only by the given flow conditions, but also by the thermodynamic state of gases. This means that when a gas slip occurs in a general gas system, the gas in the system can undergo either a dilute gas flow at a small Knudsen number or a dense gas flow at a relatively large Knudsen number. In addition, it is also found from Fig. 8 that the difference between the outlet slip velocity of a dilute gas and that of a dense gas increases with the Knudsen number. Specifically, comparing the outlet slip velocity for σ/δ=0.5 with that for σ/δ=0.1, it is found the difference of the outlet slip velocities in these two cases increases by 88% when the Knudsen number increases from 0.01 to 0.04. This increased deviation indicates that the dense effect caused by a large length ration σ/δ on gas dynamics becomes more noticeable in the large Knudsen number flows. In summary,

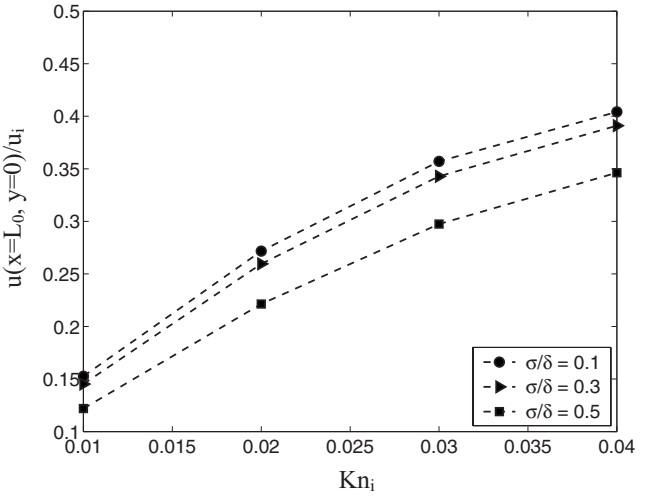

FIG. 8. The dependence of slip velocity on the Knudsen number with different σ/δ.

based on the above observations, we can conclude that dense gas flows with a large length ratio σ/δ present quite different dynamic behaviors from dilute gas flows do even under the same flow conditions.

V. CONCLUSIONS

Gas flows in microchannels is usually assumed to be dynamically similar to rarefied gas flows at high altitudes, and is characterized by the Knudsen number. However, in many practical cases this basic assumption is questionable, and the dense effect should be considered. In this paper, we have presented a finite difference LBGK model based on the Enskog equation for dense gases, and have applied the model to study several dense gas flows in microchannels. The numerical results show that dense gas flows in microchannels present an apparent slip on the solid wall when the Knudsen number is in the order of 10^{-2}, and the magnitude of such a slip depends on the length ratio σ/δ of gas: a larger length ratio σ/δ results in a smaller slip velocity on the solid wall. Moreover, the numerical results show different σ/δ also changes the fluid velocity profile and pressure distribution in the bulk flow region. These results demonstrate that dense gas flows in microchannels with a large σ/δ behave differently from dilute gas flows in microchannels with a small σ/δ. Therefore, a simple treatment of all gas flows in microchannels as rarefied gas flows (i.e., the dilute gas flows with a finite Knudsen number) will result in an inaccurate prediction of the flow behaviors.

ACKNOWLEDGMENTS

This work was supported by a grant from the Research Grants Council of the Hong Kong Special Administrative Region, China (Project No. HKUST6101/04E)

[1] G. E. Karniadakis and A. Beskok, *Micro flows: Fundamental and Simulations* (Springer-Verlag, New York, 2002).
[2] C. Shen, *Rarefied Gas Dynamics: Fundamentals, Simulation and Micro Flows* (Springer-Verlag, Berlin, 2005).
[3] H. S. Tsien, J. Aeronaut. Sci. **13**, 653 (1946).
[4] G. A. Bird, *Molecular Gas Dynamics and the Direct Simulation of Gas Flows* (Clarendon Press, Oxford, 1994).
[5] S. Chapman and T. G. Cowling, *The Mathematical Theory of Non-uniform Gases: An Account of the Kinetic Theory of Viscosity, Thermal Conduction and Diffusion in Gases* (Cambridge University Press, Cambridge, 1990).
[6] H. Xue and S. Chen, Microscale Thermophys. Eng. **7**, 69 (2003).
[7] M. Wang and Z. Li, Phys. Rev. E **68**, 046704 (2003).
[8] F. Yan and B. Farouk, Microscale Thermophys. Eng. **6**, 235 (2002).
[9] K. Xu and Z. Li, J. Fluid Mech. **513**, 87 (2004).
[10] X. Nie, G. D. Doolen, and S. Chen, J. Stat. Phys. **107**, 279 (2002).
[11] X. Y. He, Q. S. Zou, L. S. Luo, and M. Dembo, J. Stat. Phys. **87**, 115 (1997).
[12] C. Y. Lim, C. Shu, X. D. Niu, and Y. T. Chew, Phys. Fluids **14**, 2299 (2002).
[13] S. Succi, Phys. Rev. Lett. **89**, 064502 (2002).
[14] T. Lee and C. L. Lin, Phys. Rev. E **71**, 046706 (2005).
[15] S. Ansumali and I. V. Karlin, Phys. Rev. E **66**, 026311 (2002).
[16] G. H. Tang, W. Q. Tao, and Y. L. He, Phys. Fluids **17**, 058101 (2005).
[17] Z. L. Guo, T. S. Zhao, and Y. Shi, J. Appl. Phys. **99**, 074903 (2006).
[18] W. T. Kim, M. S. Jhon, Y. Zhou, I. Staroselsky, and H. Chen, J. Appl. Phys. **97**, 10P304 (2005).
[19] S. C. Kang, R. M. Crone, and M. S. Jhon, J. Appl. Phys. **85**, 5594 (1999).
[20] X. Y. He and L. S. Luo, Phys. Rev. E **55**, R6333 (1997).
[21] X. Y. He and L. S. Luo, Phys. Rev. E **56**, 6811 (1997).
[22] Y. Shi, T. S. Zhao, and Z. L. Guo, Phys. Rev. E **73**, 026704 (2006).
[23] J. O. Hirschfelder, C. F. Curtiss, and R. B. Bird, *Molecular Theory of Gases and Liquids* (John Wiley & Sons, New York, 1964).
[24] L. S. Luo, Phys. Rev. Lett. **81**, 1618 (1998).
[25] L. S. Luo, Phys. Rev. E **62**, 4982 (2000).
[26] H. Schlichting and K. Gersten, *Boundary-Layer Theory* (Springer-Verlag, Berlin, 2000).
[27] Y. H. Qian, D. D'Humières, and P. Lallemand, Europhys. Lett. **17**, 479 (1992).
[28] Z. L. Guo, C. Zheng, and T. S. Zhao, J. Sci. Comput. **16**, 569 (2001).
[29] P. Lallemand and L. S. Luo, Phys. Rev. E **68**, 036706 (2003).
[30] G. R. McNamara, A. L. Garcia, and B. J. Alder, J. Stat. Phys. **81**, 395 (1995).
[31] V. Sofonea and R. F. Sekerka, J. Comput. Phys. **207**, 639 (2005).
[32] C. Cercignani, R. Illner, and M. Pulvirenti, *The Mathematical Theory of Dilute Gases* (Springer-Verlag, New York, 1994).
[33] Z. L. Guo, C. G. Zheng, and B. C. Shi, Phys. Fluids **14**, 2007 (2002).
[34] C. Shen, D. B. Tian, C. Xie, and J. Fan, Microscale Thermophys. Eng. **8**, 423 (2004).
[35] Z. L. Guo, C. G. Zhen, and B. C. Shi, Chin. Phys. **11**, 366 (2002).
[36] E. B. Arkilic, M. A. Schmidt, and K. S. Breuer, J. Microelectromech. Syst. **6**, 167 (1997).
[37] S. Ansumali, I. V. Karlin, C. E. Frouzakis, and K. B. Boulouchos, Physica A **359**, 289 (2006).
[38] S. Chen, D. Martínez, and R. Mei, Phys. Fluids **8**, 2527 (1996).